Microchimica Acta (2019) 186: 397
https://doi.org/10.1007/s00604-019-3491-9

ORIGINAL PAPER

A nanocomposite prepared from copper(II) and nitrogen-doped graphene quantum dots with peroxidase mimicking properties for chemiluminescent determination of uric acid

Bingfang Shi[1] · Yubin Su[2] · Yan Duan[1] · Shengyu Chen[1] · Weiyuan Zuo[1]

Received: 29 November 2018 / Accepted: 12 May 2019 / Published online: 3 June 2019

Abstract

Nitrogen-doped graphene quantum dots (N-GQD) were employed along with Cu(II) ions under alkaline conditions and room temperature to synthesize nanocomposites of type Cu(II)/Cu_2O/N-GQDs. These nanocomposites exhibit excellent stability and dispersity, and also display a peroxidase-like activity that is superior to pure Cu_2O nanoparticles and natural peroxidase (POx). A chemiluminescence (CL) method was designed that is based on the use of uricase which oxidizes uric acid under formation of H_2O_2. The nanocomposites were used as a POx mimic in the luminol-H_2O_2 CL system. Under optimized conditions, a linear relationship between CL intensity and the uric acid (UA) concentration in the range of 0.16—4.0 μM, and a detection limit of 0.041 μM (at S/N = 3) were obtained. The CL method was applied to the determination of UA in spiked serum and urine, and recoveries ranged from 85.0 to 121.3%.

Keywords Chemiluminescence · Nanocomposite · Molecule detection · Urine

Introduction

Uric acid (UA), as an oxidation end product, is produced in human physiological fluids of serum and urine during the purine metabolism [1]. UA may accumulate in the human body despite its low solubility. High levels of UA in the body can be indicative of several diseases such as gout, high cholesterol, cardiovascular diseases and kidney diseases [2, 3]. UA level in the body can be adopted as a factor for health assessment and disease diagnosis. Therefore, it is significant to monitor the level of UA in body fluid with high accuracy and sensitivity.

Various techniques have been proposed and employed to detect UA, such as potentiometric [4], fluorescence [5], colorimetric [6], and enzymatic [7], but the applications of these methods are limited because of their shortcomings, that include sophisticated instrumentation and equipment, expensive enzymes, complicated sample preparation processes, and time-consuming immobilizing processes [7]. Electrochemical detection of UA has received considerable attention because the process is simple, inexpensive, provides high sensitivity and selectivity, and is rapid [8]. However, the main drawback of electrochemical determination of UA is that the process finds it difficult to discriminate the oxidation potential of UA from interfering substances in body fluids. Hence, cost-effective, rapid and simple method with high sensitivity is required for the determination of UA.

Chemiluminescence (CL), as an effective and simple strategy, that exhibits the advantages of high sensitivity, low background interference, and simple instrumentation, and has been exploited with broad applications in the analytical field [9, 10]. Among the common reagents used in CL reaction, the luminol-H_2O_2 system plays a vital role in a wide range of applications, which has to be catalyzed by horseradish peroxidase (HRP), DNAzyme, and metal ions [11, 12]. Unfortunately, these types of catalysts still have drawbacks, such as low stability for peroxidases, a complicated

Electronic supplementary material The online version of this article (https://doi.org/10.1007/s00604-019-3491-9) contains supplementary material, which is available to authorized users.

✉ Bingfang Shi
shibingfang@126.com

[1] Key Laboratory of Regional Ecological Environment Analysis and Pollution Control of West Guangxi, College of Chemistry and Environmental Engineering, Baise University, Baise 533000, China

[2] State Key Laboratory for the Chemistry and Molecular Engineering of Medicinal Resources, School of Chemistry and Pharmaceutical Sciences, Guangxi Normal University, Guilin 541004, China

modification for DNAzyme, and high toxicity for metal ions. To significantly improve the analytical performance of CL methods, much attention has been given on using nanomaterials (including metal nanoclusters [13], metallic oxide nanoparticle [14], metal-organic frameworks [15], graphene oxide [16, 17], and graphene-metallic oxide nanocomposite [18]) as catalysts to strengthen the CL emission and enhance the inherent sensitivity.

Copper (I) oxide nanoparticles (Cu_2O NPs), as an excellent *p*-type semiconductor material, has attracted extensive attention due to its excellentunique optical, hypertoxicity, electric, and catalytic properties [19]. Cu_2O, which possesses intrinsic peroxidase-like activities, can be used to catalyze the luminol-H_2O_2 CL system by decomposing H_2O_2 to yield active radicals [20]. However, the catalytic activity of Cu_2O NPs rapidly degrades due to dissolution and agglomeration [21]. Hence, various supports including carbon NPs and polymers have are appointed to maximize the stability and catalytic activity of Cu_2O NPs. Synthesis of the nanocomposite is described in detail in the Electronic Supporting Material (ESM). These new approaches have been successful in synthesizing Cu_2O@carbon nanocomposites, and electronic conductivity improved significantly. Specifically, the synthesis of Cu_2O@carbon nanocomposite requires not only rigorous synthesis temperature but much complex and time-consuming synthesis steps, as well as the addition of a toxic reducing agent. Additionally, most of the support materials for the preparation of Cu_2O@carbon nanocomposites by the aforementioned approaches are carbon dots or reduced graphene. Some researchers demonstrated that nitrogen doped grapheme quantum dots (N-GQDs) acted as advanced support materials due to their large specific surface area and excellent electrocatalytic properties [22]. Much less attention has been given towards a rapid, environmentally friendly, with suitable working temperature (room temperature), and reducing agent-free strategy for the synthesis of Cu_2O@N-GQDs.

We introduce here a room-temperature and reducing agent-free strategy for the preparation of Cu(II)/Cu_2O nanoparticle/nitrogen-doped graphene quantum dot hybrids (Cu(II)/Cu_2O/N-GQDs). During the synthesis of N-GQDs, citric acid was used as the carbon source and 3,4-dihydroxy-L-phenylalanine as dopant, respectively. Cu(II)/Cu_2O/N-GQDs were then facially synthesized via in situ reductions of Cu^{2+} in N-GQD solution under alkaline conditions at room temperature (Scheme 1). Moreover, the Cu(II)/Cu_2O/N-GQDs can resist extreme pH and temperatures. Specifically, because of N-GQDs employed as reducing agents and support materials, the Cu(II)/Cu_2O/N-GQDs exhibit good dispersity and outstanding peroxidase-like catalytic properties. Based on these, a CL method based on Cu(II)/Cu_2O/N-GQDs was developed for the sensitively and selectively determination of uric acid (UA). This CL method was further applied for detection of UA in human serum and urine samples.

Experimental

Materials

Uric acid (UA, 99%), urate oxidase, superoxide dismutase, luminol, and l-3-(3,4-Dihydroxyphenyl) alanine (L-DOPA, 98%) were obtained from Sigma Aldrich Co., Ltd. (http://www.vvchem.com/, United Kingdom). Citric acid (99.5%), hydrogen peroxide (H_2O_2, 30%, *v*/v), superoxide dismutase (SOD), sodium ascorbate, $CuCl_2$, Na_3PO_4, Na_2HPO_4, methanol, L-ascorbic acid, NaH_2PO_4, NaOH and HCl were purchased from Aladdin Chemistry Co., Ltd. (https://www.chemicalbook.com/, Shanghai, China). All reagents are of analytical grade and were used without further purification. Ultrapure water was prepared using a Millipore water purification system (18 MΩ·cm, Milli-Q, Millipore) and was used in all of the runs.

Preparation of nitrogen-doped graphene quantum dots (N-GQDs)

N-GQDs were prepared using citric acid as the carbon source and L-DOPA as the N source through a solid phase thermal treatment according to our previous work [23]. Briefly, citric acid (1.0 g) and L-DOPA (1.0 g) were placed in a glass cuvette and heated at 230 °C for 40 min under vigorous stirring. After the reaction was complete, the obtained orange mixture was cooled to room temperature naturally and dissolved in 10 mL of ultrapure water by ultrasonic agitation. Then, the pH of the obtained mixed solution was adjusted to neutral by adding 1 M of NaOH drop by drop. The mixture was dialyzed with a dialysis membrane (MW = 1 kD) for 24 h to remove impurities and residual reagents. After dialysis, the aqueous solution was dried using a freeze dryer, and the obtained product was stored at 4 °C for later characterization and further use.

Preparation of Cu(II)/Cu_2O/N-GQDs

Cu(II)/Cu_2O/N-GQDs were synthesized by $CuCl_2$ and N-GQDs under alkaline conditions at room temperature. 300 μL of the N-GQD solution (12.2 $mg{\cdot}mL^{-1}$), 40 μL of NaOH solution (1 M) and 160 μL of $CuCl_2$ (0.5 M) solution were mixed and sonicated for 20 min at room temperature. Subsequently, the obtained solution was centrifuged and washed three times. After that, the obtained solid matter was dried using a freeze dryer and stored at 4 °C for characterization and further use.

For comparison, Cu_2O nanoparticles were also synthesized according to a previous report [24]. Briefly, 1 mL of NaOH (0.35 M) was quickly added to 30 mL of $CuCl_2$ solution (0.0032 M) under vigorous stirring and argon atmosphere. Then, the sodium ascorbate solution was added into the

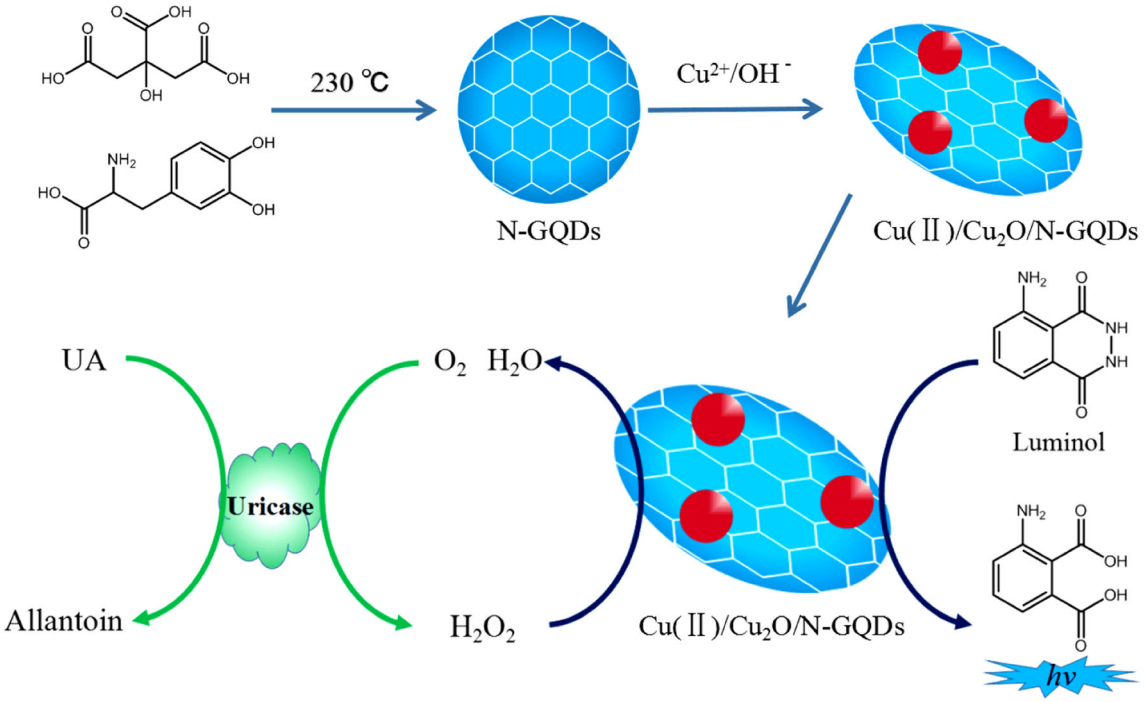

Scheme 1 Synthesis strategy of Cu(II)/Cu_2O/N-GQDs and the CL method based Cu(II)/Cu_2O/N-GQDs for H_2O_2-meidated uric acid detection.

solution drop-wise at room temperature. The color of the solution changed from blue to brick-red, indicating the formation of Cu_2O. The obtained brick-red precipitates were washed three times with distilled water and absolute ethanol, respectively. The final samples were stored in an Ar atmosphere after being dried in vacuum at 45 °C and stored at 4 °C for further use.

Instrumentation

A Cary 60 UV-vis spectrometer (Agilent Technologies, USA) was used for absorption measurements. The chemiluminescence spectra were monitored using a Cary Eclipse Fluorescence spectrophotometer (Agilent Technologies, USA) under the optimal conditions: voltage of 750 V and emission slit of 10 nm, respectively. Fourier transform infrared (FT-IR) spectroscopy (4000–400 cm^{-1}) study was conducted from KBr pellets on a Perkin-Elmer FT-IR spectrophotometer (Perkin-Elmer, USA). Transmission electron microscopy (TEM) were carried out using a Tecnai G2 F20TEM (FEI, USA) operating at 200 kV. X-Ray photoelectron spectra (XPS) were performed with a Thermo ESCALAB 250Xi Multitechnique Surface Analysis (Thermo, USA). X-ray diffraction (XRD) analyses were conducted on a RigakuD/max 2500 v/pc X-ray powder diffractometer (Rigaku, Japan) with Cu K_α radiation (λ = 0.154 nm).

Chemiluminescence (CL) method for H_2O_2 and uric acid (UA) detection

In a typical experiment, 10 μL of Cu(II)/Cu_2O/N-GQDs (0.07 mg·mL^{-1}) and 10 μL of luminol (0.8 mM) was added in 970 μL of phosphate buffer (250 mM, pH = 9.0). Then, 10 μL of H_2O_2 with concentrations of 0.4, 0.8, 1.0, 2.0, 4.0, 8.0, 10.0, 20.0 and 40.0 μM were added to the above mixture, respectively. The CL was recorded immediately, and the emission intensity at 422 nm was used to evaluate the assay performance.

For the detection of UA, 16 μL of urate oxidase (2.5 U·μL^{-1}) was incubated with 10 μL UA (the concentration of UA was 0, 0.16, 0.24, 0.32, 0.8, 1.6, 2.4, 3.2 and 4.0 μM, respectively) at 37 °C for 40 min. Then, the obtained solution was added to the mixture, that contained 10 μL of Cu(II)/Cu_2O/N-GQDs (0.07 mg·mL^{-1}), 954 μL of phosphate buffer (250 mM, pH = 9.0) and 10 μL of luminol (0.8 mM). The chemiluminescence generated at 422 nm was used to evaluate the assay performance.

To explore the mechanism of the Cu(II)/Cu_2O/N-GQDs complex-base luminol-H_2O_2 CL system, the effects of different radical scavengers were investigated. 20 μM H_2O_2 and 0.07 mg/mL Cu(II)/Cu_2O/N-GQDs were mixed with methanol (10%, as hydroxyl radical scavenger), superoxide dismutase (SOD) (15 U, as superoxide anion scavenge), and L-ascorbic acid (3 mg·mL^{-1}). Then, 950 μL of the mixture was transferred to a cuvette and mixed with 50 μL of 0.8 mM luminol. Immediately, CL signals were monitored according to the same procedure as mentioned above.

All the measurements in this section were performed three times, and the standard deviation was plotted as the error bar.

CL method for the detection of UA in real samples

To evaluate the practicality of the presented CL method, CL method based Cu(II)/Cu_2O/N-GQDs was applied to determine the level of UA in human serum and urine sample obtained from the No. 5 hospital of Guilin (Guangxi, China). The serum and urine were filtered through a 0.22 μm membrane and centrifuged at 3000 rpm for 5 min. These samples were diluted in a 1: 1000 (*v*/v) ratio with phosphate buffer (250 mM, pH 9.0) and analyzed for UA content in them. A separate aliquot of the samples was spiked with standard solutions containing different concentrations of UA and analyzed by the CL method based Cu(II)/Cu_2O/N-GQDs.

Results and discussion

Choice of materials

N-GQDs were prepared by solid-phase pyrolysis using CA as the carbon source and L-DOPA as the nitrogen source. Most importantly, for the presence of oxygen-rich and nitrous groups on the surface of N-GQDs, N-GQDs can be used as an efficient reducing agent [23].

Recent studies demonstrated that the size of nanoparticles had been downsized resulting in enhancement of the catalytic activity of nanoparticles [25]. However, the sizes of reported Cu_2O on the surface of support materials mentioned above are 80–100 nm [26], 5 μm [27], 223 ± 8 nm [28], and 500 nm [29], respectively. Here, N-GQDs were employed along with Cu(II) ions to synthesize nanoscale Cu(II)/Cu_2O/N-GQDs with peroxidase mimicking properties.

Characterization of the N-GQDs and Cu(II)/Cu_2O/N-GQDs

The UV-vis spectra of N-GQD solution portrayed in Fig. 1a displayed two absorption peaks at 280 nm and 340 nm, which were related to the $\pi \rightarrow \pi^*$ transition of aromatic π system in N-GQDs and $n \rightarrow \pi^*$ transition of C=O bond. The XPS spectrum (Fig. S1a) confirmed that N atoms were doped successfully. Moreover, TEM images were used to characterize the morphology of the N-GQDs. As shown in Fig. 2a, most of the N-GQDs had spherical nanostructure. A lattice spacing of 0.21 nm was observed in the high-resolution TEM (HRTEM) image, which is consistent with the (110) facet of graphitic carbon [30]. Cu(II)/Cu_2O/N-GQDs were then synthesized using N-GQDs as reducing agent to in-situ reduce Cu^{2+} and form Cu_2O on the surface of the N-GQDs. As it can be seen in Fig. 1, Cu(II)/Cu_2O/N-GQDs had a absorption band that appeared at 488 nm, which is attributed to the characteristic absorption of Cu_2O nanostructure (<100 nm) [31]. A peak at 280 nm was due to the impact of N-GQDs. The obtained Cu(II)/Cu_2O/N-GQDs solution changed to brick red color (Fig. 1a, inset), which further suggested that Cu^{2+} was reduced to Cu_2O.

To further investigate the formation of Cu_2O, XPS spectra of Cu(II)/Cu_2O/N-GQDs was conducted. In Fig.S1b, it can be seen that Cu 2p peaks at about 934.9 demonstrated the presence of Cu element in the finally obtained Cu(II)/Cu_2O/N-GQDs. The high-resolution Cu 2p XPS spectra of Cu(II)/Cu_2O/N-GQDs in Fig.1b showed Cu $2p_{3/2}$ and Cu $2p_{1/2}$ peaks at about 932.5 and 953.9 eV with two shake-up satellite peaks at 940.0 and 962.5 eV, indicating the Cu^+ in the formed Cu_2O [11]. The peaks at 934.1 and 953.9 eV with shake-up satellite at 940–946 eV, which arose from electron-correlation effects in the open Cu 3d shell ($3d^9$), are corresponding to the characteristic features of Cu(II) $2p_{3/2}$ and $2p_{1/2}$ [29]. Therefore, the Cu 2p XPS spectrum of Cu(II)/Cu_2O/N-GQDs agreed with a mixed phase of Cu(II) and Cu_2O.

The TEM image of Cu(II)/Cu_2O/N-GQDs is represented in Fig.2b. The size distribution data (Fig. S2b) revealed that the average size of Cu(II)/Cu_2O/N-GQDs was about 4.5 nm, which was much smaller than that in the reported literature [26–29]. The sizes of Cu(II)/Cu_2O/N-GQDs were bigger than that of the N-GQDs (2.4 nm, Fig. S2a). A possible reason is that Cu^{2+} is prone to coordinate with oxygen-containing surface groups of N-GQDs, which facilities electron transport between N-GQDs and Cu^{2+}, resulting in the reduction of Cu^{2+}. As a result, Cu_2O NPs grew in situ on the surface of N-GQDs. At the same time, in the HRTEM image (Fig.2b, inset), the lattice of N-GQDs can only be observed in few areas, which may attribute to the formation of the Cu_2O on the surface of the N-GQDs. Fig. S3 shows the AFM images of the N-GQDs and Cu(II)/Cu_2O/N-GQDs. As shown in Fig. S3, the average thickness of the Cu(II)/Cu_2O/N-GQDs (20.1 nm, Fig. S3b) was larger than that of N-GQDs (5.6 nm, Fig. S3a), which further suggests that Cu_2O was formed and decorated on the N-GQDs surface. The results suggest that the size of Cu(II)/Cu_2O/N-GQDs could be controlled by N-GQDs. The detailed XRDs of Cu(II)/Cu_2O/N-GQDs are described in Fig. S4.

To investigate the reduction of Cu^{2+} by N-GQDs, the change of functional groups on the surface of N-GQDs and Cu(II)Cu_2O/N-GQDs were investigated by FTIR. As shown in Fig. S5, the characteristic features of N-GQDs are the absorption bands at 3414, 1703, 1458, and 1051 cm^{-1}corresponding to -OH, $-NH_2$, COO^-, and C-O stretching vibrations, respectively. Compared to the FTIR spectrum of the N-GQDs, the intensity of the -OH groups at 3414 cm^{-1} decreased. The band at 1116 cm^{-1} is attributed to the O-H stretching vibration. It disappears in the FTIR of the Cu(II)/Cu_2O/N-GQDs. The intensity of the νs_{COO-} band at 1452 cm^{-1} increases compared to the C-H

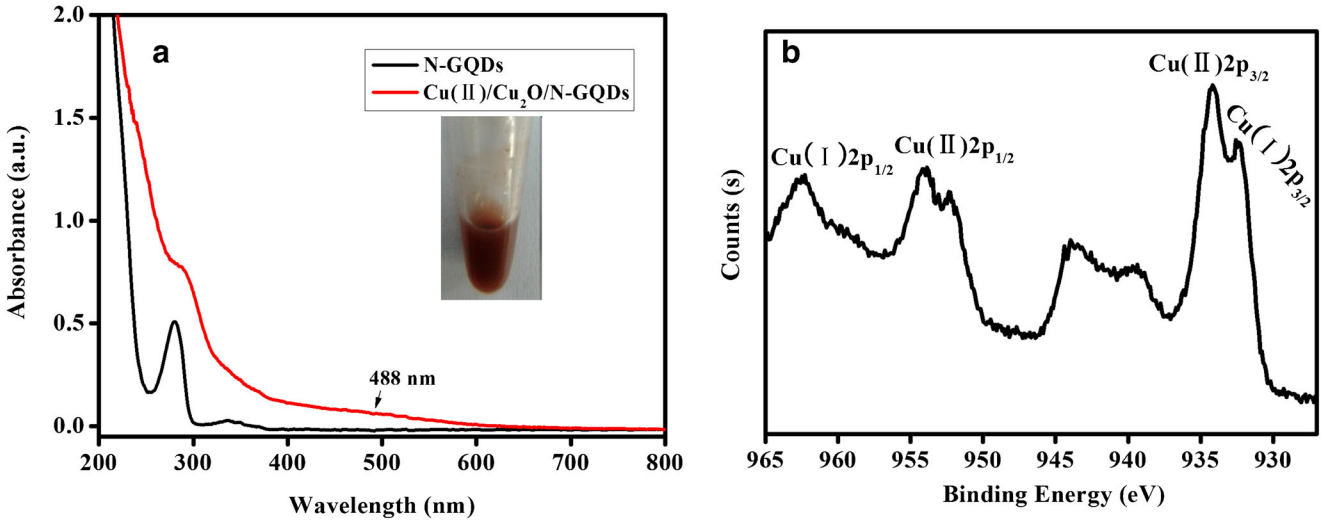

Fig. 1 The UV-vis spectrum of N-GQDs and Cu(II)/Cu_2O/N-GQDs. Inset is the photo of Cu(II)/Cu_2O/N-GQDs solution

stretching vibration at 1387 cm^{-1}. These observations suggested that the –OH groups on the surface of N-GQD were oxidized into the –COOH groups by Cu^{2+}.

To further study the change of functional groups on the nanoparticle surface, the XPS spectra of N-GQDs and Cu(II)/Cu_2O/N-GQDs were performed. In Fig. 3, Both C1s XPS spectra (Fig. 3a, b) can be divided into five peaks at 287.7, 285.5, 284.7, 284.1, and 283.5 eV, which can be assigned to C(O)-O, C=O, C-O/C-N, C-C/C=C, and C-H, respectively [32]. In comparison with the intensity of the C-H peak, a relative increase in the intensity of C(O)-O, C=O and C-O can be seen obviously in the C 1 s XPS spectra of Cu(II)/Cu_2O/N-GQDs than those of N-GQDs, which might be due to the oxidation of C-OH on N-GQDs surface by Cu^{2+}. The O1s XPS spectra of N-GQDs displayed three peaks at 532.3, 531.2, and 530.5 eV (Fig. 3c), which were attributed to O=C-O, O=C, and O-C, respectively. In the O1s XPS spectra of Cu(II)/Cu_2O/N-GQDs, a new peak located at 531.5 eV was observed (Fig. 3d) which was attributable to the lattice oxygen of Cu_2O [20]. N1 s XPS spectra of N-GQDs (a) and Cu(II)/Cu_2O/N-GQDs are shown in Fig. S6.

Peroxidase-like activity of Cu(II)/Cu_2O/N-GQDs

Based on the peroxidase-like activity of the most metal oxide NPs, whether the Cu(II)/Cu_2O/N-GQDs possess the peroxidase-like activity was investigated. As shown in Fig. S7, there was a clear absorption band at 420 nm, which belonged to the characteristic absorption peak oxidation product of ABTS [33]. At the same time, the green color solution can be observed in the presence of Cu(II)/Cu_2O/N-GQDs. These observations illustrated Cu(II)/Cu_2O/N-GQDs showing an intrinsic peroxidase-like activity.

To further elucidate the performance of the Cu(II)/Cu_2O/N-GQDs for the catalytic oxidation of ABTS by H_2O_2, the catalytic ability of N-GQDs, Cu^{2+}, Cu_2O and mixing N-GQDs, Cu_2O and Cu^{2+} were also investigated. As shown in Fig. S7, under the same conditions, the intensity of band at 420 nm generated by N-GQDs, Cu^{2+}, Cu_2O and mixing N-GQDs, Cu_2O and Cu^{2+} was less than that produced by Cu(II)/Cu_2O/N-GQDs, indicating Cu(II)/Cu_2O/N-GQDs with a small diameter exhibiting superior peroxidase-like activity towards the catalytic oxidation of ABTS by H_2O_2. The absorbance

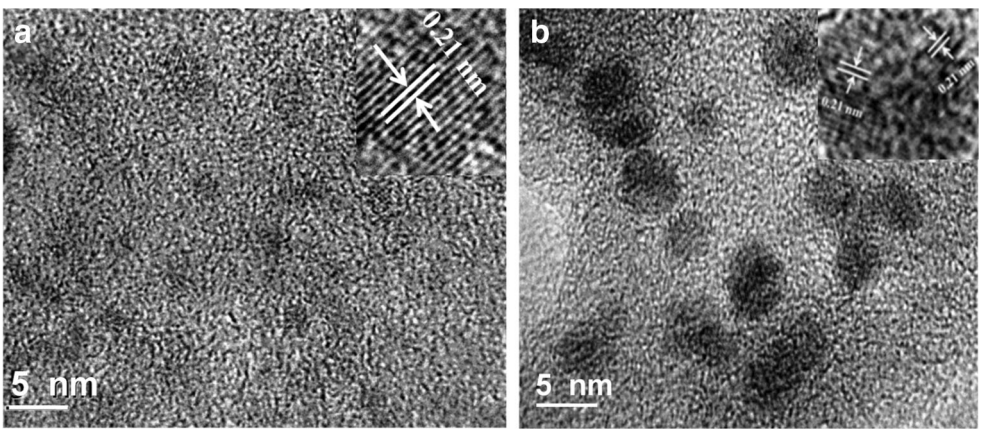

Fig. 2 TEM images and HRTEM (inset) of the N-GQDs (**a**) and the Cu(II)/Cu_2O/N-GQDs (**b**)

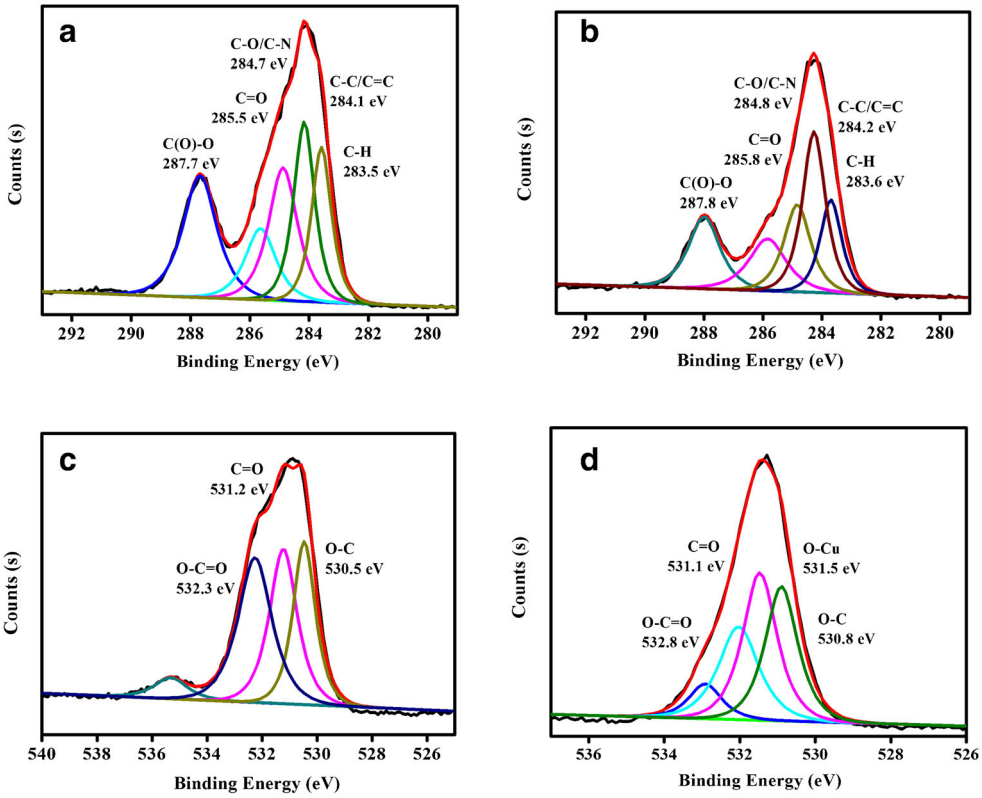

Fig. 3 C1s (**a**) and O1s (**c**) XPS spectra of N-GQDs; C1s (**b**) and O1s (**d**) XPS spectra of Cu(II)/Cu_2O/N-GQDs

intensity generated by Cu(II)/Cu_2O/N-GQDs was less than that produced by Fe_3O_4/N-GQDs, suggesting a low catalytic efficiency of the Cu(II)/Cu_2O/N-GQDs compared to that of the Fe_3O_4/N-GQDs (Fig. S8).

It was reported that the activity of horseradish peroxidase dramatically declined after incubation at temperatures higher than 40 °C for 2 h or at pH values less than 5.0 [34]. Excitingly, the catalytic efficiencies of Cu(II)/Cu_2O/N-GQDs change little even after treatment at a range of pH values (5.0–11.0) (Fig.S9a) and temperatures (10–90 °C) (Fig.S9b). These observations confirmed that the Cu(II)/Cu_2O/N-GQDs were more stable than HRP. Moreover, in most cases, the Cu(II)/Cu_2O/N-GQDs had a better catalytic performance than HRP.

Chemiluminescence mechanism of luminol-H_2O_2 catalyzed by Cu(II)/Cu_2O/N-GQDs

As shown in Fig. S10, a significant increase in the CL intensity of the luminol-H_2O_2 system at 422 nm was observed in the presence of Cu(II)/Cu_2O/N-GQDs, which belonged to the characteristic emission peak of an oxidation product of luminol. To investigate the CL mechanism of luminol-H_2O_2catalyzed by Cu(II)/Cu_2O/N-GQDs, as a proof-of-concept, SOD, methanol, and L-ascorbic acid, were added into the luminol-H_2O_2-Cu(II)/Cu_2O/N-GQDs system. As shown in Fig. S11, 68.3% and 76.5% of CL intensities were inhibited by the addition of 10% methanol (as hydroxyl radical scavenger) and 15 U SOD (as superoxide anion scavenger), respectively. Above mentioned observations indicated that superoxide radical ($O_2^{\bullet-}$) and hydroxyl radical (•OH) played pivotal roles in the process of luminol-H_2O_2reaction catalyzed by Cu(II)/Cu_2O/N-GQDs. Additionally, the CL intensity of luminol-H_2O_2-Cu(II)/Cu_2O/N-GQDs system was significantly inhibited by the addition of 3 mg·mL^{-1} L-ascorbic acid. These might have occurred due to the redox reaction between the L-ascorbic and reactive oxygen species. Hence, it can be speculated that more •OH radicals were generated in Cu(II)/Cu_2O/N-GQDs catalyzed luminol-H_2O_2 CL reaction, while $O_2^{\bullet-}$ might be generated from dissolved oxygen.

Inspired by the above results, the possible CL mechanism of luminol-H_2O_2 catalyzed by Cu(II)/Cu_2O/N-GQDs is schematically illustrated in Fig.4 and Fig. S12. The Cu(II)/Cu_2O/N-GQDs catalyzed the H_2O_2 and O_2 to generate reactive oxygen species like •OH and $O_2^{\bullet-}$. The N-GQDs used here could enhance the electronic conductivity of the Cu(II)/Cu_2O/N-GQDs, which may facilitate the catalysis reaction for the generation of reactive oxygen species. The produced •OH and $O_2^{\bullet-}$ reacted with luminol anion to generate endoperoxide, which was unstable and rapidly decomposed into excited 3-aminophthalate anion. The excited 3-aminophthalate anion would be returned to the ground state emitting the light at 422 nm.

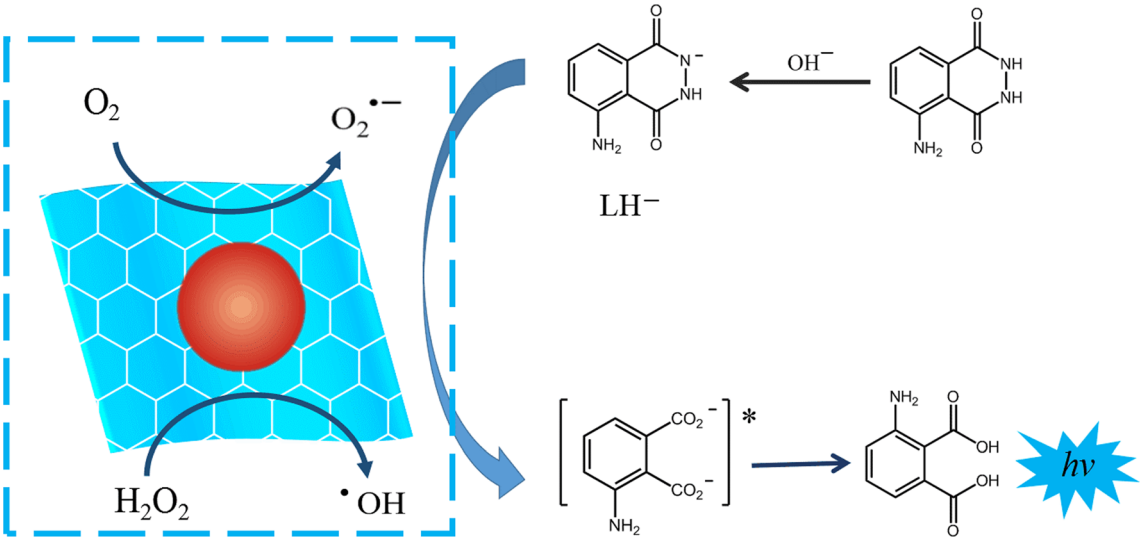

Fig. 4 Possible chemiluminescence mechanism of luminol-H_2O_2catalyzed by Cu(II)/Cu_2O/N-GQDs

Chemiluminescence assay for H_2O_2

To evaluate the performance of Cu(II)/Cu_2O/N-GQDs-luminol-H_2O_2 system for H_2O_2 detection, several important reaction conditions including pH, the concentration of Cu(II)/Cu_2O/N-GQDs and luminol were optimized. As shown in Fig. S13, the optimal pH, Cu(II)/Cu_2O/N-GQDs concentration, and luminol concentration were found to be 9.0, 0.07 mg·mL^{-1}, and 0.8 mmol·L^{-1}, respectively.

Under the optimal conditions, CL biosensor based Cu(II)/Cu_2O/N-GQDs for the detection of H_2O_2 were conducted. As illustrated in Fig. 5a, the CL intensity was increased with increasing H_2O_2 concentrations. There was a good linear correlation between the CL intensity at 422 nm and the H_2O_2 concentration in the range of 0.4–10.0 μM (Fig.5b). The linear equation is $I = 49.93C - 35.91$, with $R^2 = 0.995$, where the I stands for the CL intensity of the system, C stands for the different concentrations of H_2O_2, and it was estimated that the detection limit was as low as 0.11 μM, when signal to noise ratio (S/N) was 3 (and inset). These results demonstrated that the CL method based Cu_2O/Cu_2O/N-GQDs have an excellent potential for detection of H_2O_2.

Chemiluminescent determination of uric acid

It is well-known that UA can be oxidized by uricase to produce H_2O_2. Hence, a sensitive method to detect UA through the H_2O_2-mediated oxidation reaction by Cu(II)/Cu_2O/N-GQDs-based CL method was proposed. Before the detection of UA, it is necessary to optimize the

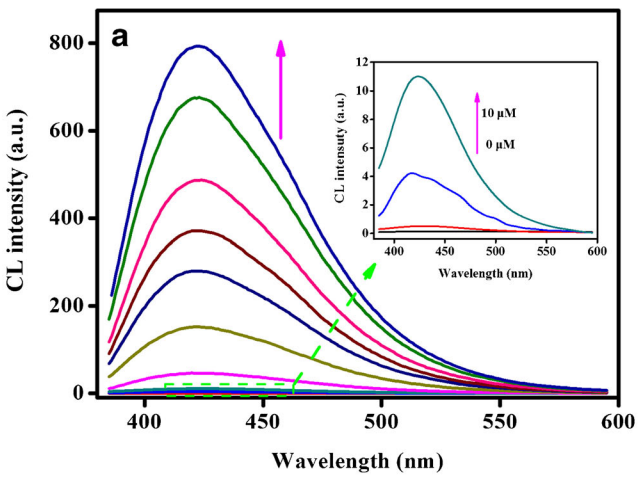

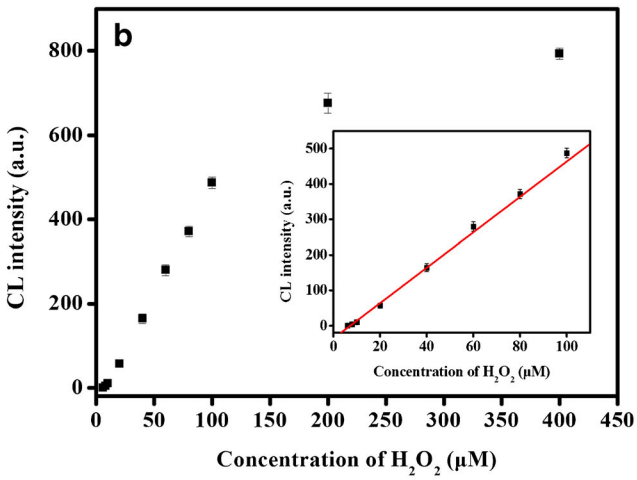

Fig. 5 CL spectra of Cu(II)/Cu_2O/N-GQDs nanocomposite-based CL method in the presence of different concentrations of H_2O_2. The concentrations of H_2O_2 from down to top were 0, 0.4, 0.8, 1.0, 2.0, 4.0, 8.0, 10.0, 20.0 and 40.0 μM (**a**). The CL intensity at 422 nm versus the concentration of H_2O_2 and the inset was the linear plot of the CL intensity at 422 nm against the H_2O_2 concentration (**b**)

amount of uricase and reactive time. As shown in Fig.S14,16 μL of UA (2.5 U·ml^{-1}) and 40 min were selected for the UA detection. Different concentrations of UA were mixed with the uricase at 37 °C and reacted for 40 min; the reactive solution was added immediately in Cu(II)/Cu_2O/N-GQDs-luminol system. The intensity at 422 nm of the CL system was increased gradually with the concentration of UA increasing (Fig.6a). The CL intensity is linearly proportional to the UA concentration in the range of 0.16–4.0 μM (Fig. 6b), and the linear equation is $I = 11.8331C_{UA} - 2.6992$, with $R^2 = 0.998$, where I is the CL intensity of the system, and C_{UA} is the concentration of UA. At the same time, the detection limit was estimated to be about 0.041 μM ($S/N = 3$), which is comparable to or lower than those in previously reported CL methods (Table S1). The results indicated the high sensitivity of the CL method for UA detections.

Furthermore, to evaluate the specificity of the present work, the CL intensity of Cu(II)/Cu_2O/N-GQDs-luminol-UA/uricase system containing some irons and possible biological interferents was investigated. As it can be seen in Fig.7, even when the concentration of K^+, Ca^{2+}, glucose (Glu), urea (Ure), lactic acid (Lac), aspartic acid (Asp), glycine (Gly), cysteine (Cys), and lysine (Lys) was 40 μM, no obvious change was observed, which was in agreement with previous report [13]. It was clear that these species mentioned above did not affect the detection of UA. Unexpectedly, obvious changes were observed with the addition of Fe^{2+}, Mn^{2+}, and ascorbic acid (Asc), which suggested that Fe^{2+}, Mn^{2+}, and ascorbic acid may strongly influence UA detection performance (Fig. 7). Fig. S15 shows that the interference of the above interfering ions was eliminated by adding 0.5 mM EDTA. The interference of ascorbic acid can be circumvented by using 4-hydroxy-2,2,6,6-tetramethyl-N-oxygen-piperidine as ascorbic acid quencher. The results show promising selectivity of the CL assay based on Cu(II)/Cu_2O/N-GQDs for the detection of uric acid.

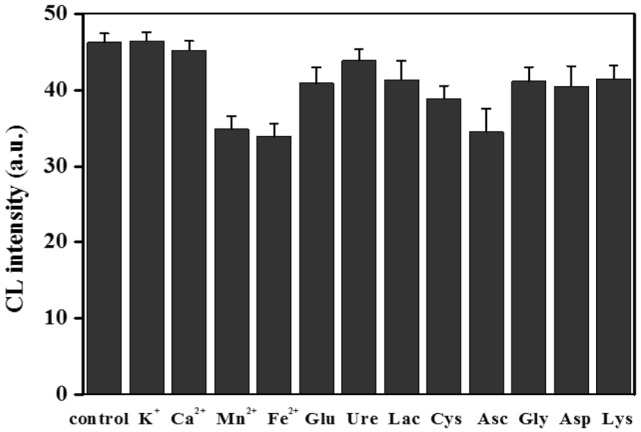

Fig. 7 Selectivity of the strategy for UA sensing. UA, K^+, Ca^{2+}, Mn^{2+}, Fe^{2+}, ascorbic acid and cysteine were at a concentration of 4.0 μM. The concentrations of other interfering substance were 40.0 μM

CL sensing of UA in biological samples

Based on the efficiency of CL method based Cu(II)/Cu_2O/N-GQDs for the sensitive and selective determination of UA, the CL method based Cu(II)/Cu_2O/N-GQDs was applied to detect UA in complex biological samples. Dilute human serum and urine samples were spiked with standard solutions with different concentrations of UA and measured by the CL method. The accuracy of the CL method was proven by the Student's t test. The Table 1 shows that the UA

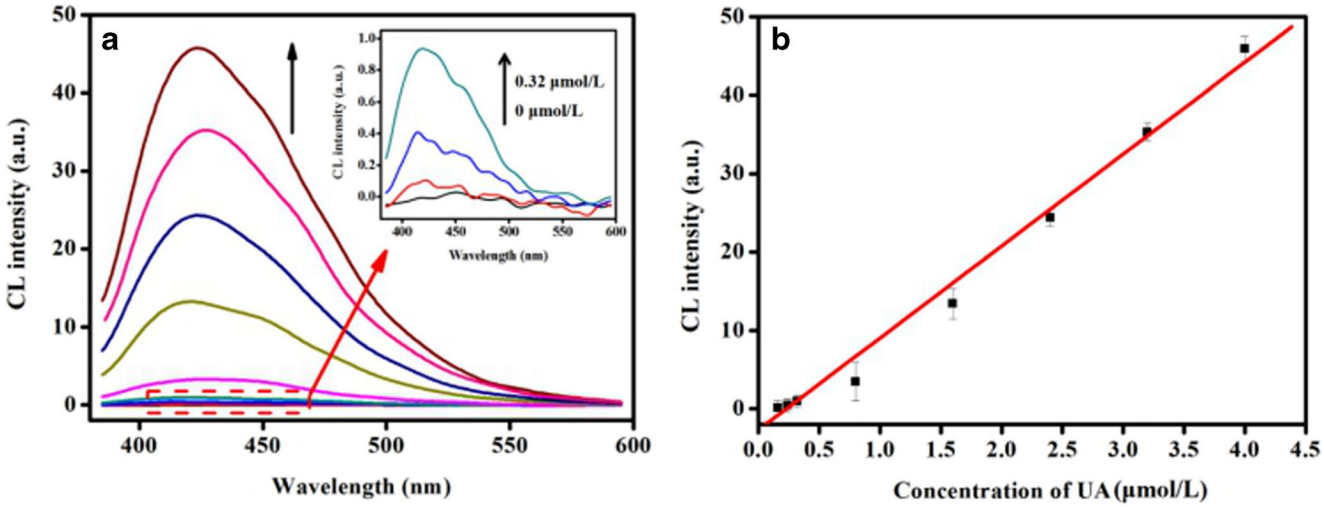

Fig. 6 CL spectra of Cu(II)/Cu_2O/N-GQDs nanocomposite-based CL method in the presence of different concentrations of UA from 0 to 4.0 μM (**a**). The linear plot of the CL intensity at 422 nm against the UA concentration (**b**)

Table 1 Measure value and recoveries of the determination of uric acid in human urine and serum samples using the CL method based Cu(II)/Cu_2O/N-GQDs

Sample	Measure value (μM)	Added (μM)	Found (μM)	t-test	P (95%)	Recovery (%)
Urine 1	2.41	0.8	3.38	5.5	0.003	121.3
Urine 2	2.56	1.0	3.47	2.6	0.047	91.0
Urine 3	2.57	1.2	3.83	4.9	0.004	105.0
Serum 1	0.21	0.4	0.68	4.8	0.005	117.5
Serum2	0.30	0.8	0.98	4.4	0.007	85.0
Serum3	0.27	1.2	1.51	3.5	0.016	103.3

contents found were insignificantly different at the 95% confidence level. The recoveries of serum and urine samples were in the range from 91.0% to 121.3% and 85.0% to 117.5%, respectively ($n = 6$). All observations further approved the reliability and feasibility of the CL method.

Conclusions

A room temperature and reducing agent-free strategy is presented for the preparation of Cu(II)/Cu_2O/N-GQDs possessing peroxidase-like activity. The Cu(II)/Cu_2O/N-GQDs exhibited excellent catalytic performance and stability over a range of pH and temperatures. These results suggested that Cu(II)/Cu_2O/N-GQDs, as peroxidase mimics, were attractive candidates for the development of a super-sensitive CL sensing method. As a consequence, a CL method for the sensitive and selective detection of UA was developed based on the luminol-H_2O_2 system using Cu(II)/Cu_2O/N-GQDs as catalysts. Considering analytical chemistry, the CL method based on Cu(II)/Cu_2O/N-GQDs enriches luminol CL mechanism, and can be further applied for the detection of important molecules.

Acknowledgements This work was financially supported by the Natural Science Foundation of China (No. 21665001).

Compliance with ethical standards The author(s) declare that they have no competing interest.

References

1. Kaur H, Halliwell B (1990) Action of biologically-relevant oxidizing species upon uric acid. Identification of uric acid oxidation products. Chem Biol Interact 73(2–3):235–247
2. Lakshmi D, Whitcombe MJ, Davis FP, Sharma S, Prasad BB (2011) Electrochemical detection of uric acid in mixed and clinical samples: a review. Electroanalysis 23(2):305–320
3. Kumar S, Bhushan P, Bhattacharya S (2016) Development of a paper-based analytical device for colorimetric detection of uric acid using gold nanoparticles- graphene oxide (AuNPs-GO) conjugate. Anal Methods 8(38):6965–6973
4. Kiran R, Scorsone E, Mailley P, Bergonzo P (2012) Quasi-real time quantification of uric acid in urine using boron doped diamond microelectrode with in situ cleaning. Anal Chem 84(23):10207–10213
5. Liu Y, Li H, Guo B, Zhang Y (2017) Gold nanoclusters as switch-off fluorescent probe for detection of uric acid based on the inner filter effect of hydrogen peroxide-mediated enlargement of gold nanoparticles. Biosens Bioelectron 91:734–740
6. Gubala V, Harris LF, Ricco AJ, Tan MX, Williams DE (2011) Point of care diagnostics: status and future. Anal Chem 84(2):487–515
7. Long Q, Fang A, Wen Y, Li H, Zhang Y, Yao S (2016) Rapid and highly-sensitive uric acid sensing based on enzymatic catalysis-induced upconversion inner filter effect. Biosens Bioelectron 86: 109–114
8. Özcan A, İlkbaş S (2015) Preparation of poly (3, 4-ethylenedioxythiophene) nanofibers modified pencil graphite electrode and investigation of over-oxidation conditions for the selective and sensitive determination of uric acid in body fluids. Anal Chim Acta 891:312–320
9. Iranifam M, Sorouraddin MH (2014) Flow injection chemiluminescence determination of naphazoline hydrochloride in pharmaceuticals. Luminescence 29(1):48–51
10. Iranifam M, Khabbaz Kharameh M (2015) Cupric oxide nanoparticles-enhanced chemiluminescence method for measurement of β-lactam antibiotics. Luminescence. 30(5):625–630
11. Cai N, Tan L, Li Y, Xia T, Hu T, Su X (2017) Biosensing platform for the detection of uric acid based on graphene quantum dots and G-quadruplex/hemin DNAzyme. Anal Chim Acta 965:96–102
12. Lu HF, Li JY, Zhang MM, Wu D, Zhang QL (2017) A highly selective and sensitive colorimetric uric acid biosensor based on Cu(II)-catalyzed oxidation of 3,3′,5,5′-tetramethylbenzidine. Sensors Actuators B Chem 244:77–83
13. Sheng Y, Yang H, Wang Y, Han L, Zhao Y, Fan A (2017) Silver nanoclusters-catalyzed luminol chemiluminescence for hydrogen peroxide and uric acid detection. Talanta 166:268–274
14. Iranifam M, Hendekhale NR (2017) CuO nanoparticles-catalyzed hydrogen peroxide-sodium hydrogen carbonate chemiluminescence system used for quenchometric determination of atorvastatin, rivastigmine and topiramate. Sensors Actuators B Chem 243:532–541
15. Luo F, Lin Y, Zheng L, Lin X, Chi Y (2015) Encapsulation of hemin in metal-organic frameworks for catalyzing the chemiluminescence reaction of the H_2O_2-luminol system and detecting glucose in the neutral condition. ACS Appl Mater Interfaces 7(21): 11322–11329
16. Tang D, Liu J, Yan X, Kang L (2016) Graphene oxide derived graphene quantum dots with different photoluminescence properties and peroxidase-like catalytic activity. RSC Adv 6(56):50609–50617
17. Lin L, Song X, Chen Y, Rong M, Zhao T, Wang Y, Ji Y, Chen X (2015) Intrinsic peroxidase-like catalytic activity of nitrogen-doped graphene quantum dots and their application in the colorimetric detection of H2O2 and glucose. Anal Chim Acta 869:89–95

18. Abdolmohammad-Zadeh H, Rahimpour E (2015) Utilizing of Ag@AgCl@graphene oxide@Fe_3O_4 nanocomposite as a magnetic plasmonic nanophotocatalyst in light-initiated H_2O_2 generation and chemiluminescence detection of nitrite. Talanta 144:769–777
19. Lee S, Liang CW, Martin LW (2011) Synthesis, control, and characterization of surface properties of Cu_2O nanostructures. ACS Nano 5(5):3736–3743
20. Huang C, Ye W, Liu Q, Qiu X (2014) Dispersed Cu_2O octahedrons on h-BN nanosheets for p-nitrophenol reduction. ACS Appl Mater Interfaces 6(16):14469–14476
21. Wang YJ, Wilkinson DP, Zhang J (2011) Noncarbon support materials for polymer electrolyte membrane fuel cell electrocatalysts. Chem Rev 111(12):7625–7651
22. Si Y, Samulski ET (2008) Exfoliated graphene separated by platinum nanoparticles. Chem Mater 20(21):6792–6797
23. Shi B, Su Y, Zhao J, Liu R, Zhao Y, Zhao S (2015) Visual discrimination of dihydroxybenzene isomers based on a nitrogen-doped graphene quantum dot-silver nanoparticle hybrid. Nanoscale 7(41):17350–17358
24. Xu Y, Wang H, Yu Y, Tian L, Zhao W, Zhang B (2011) Cu_2O nanocrystals: surfactant-free room-temperature morphology-modulated synthesis and shape-dependent heterogeneous organic catalytic activities. J Phys Chem C 115(31):15288–15296
25. Lim H, Ju Y, Kim J (2016) Tailoring catalytic activity of Pt nanoparticles encapsulated inside dendrimers by tuning nanoparticle sizes with subnanometer accuracy for sensitive chemiluminescence-based analyses. Anal Chem 88(9):4751–4758
26. Zhao Z, Wang Y, Li P, Sang S, Zhang W, Hu J, Kun Lian K (2015) A highly sensitive electrochemical sensor based on cu/Cu_2O@carbon nanocomposite structures for hydrazine detection. Anal Methods 7(21):9040–9046
27. An X, Li K, Tang J (2014) Cu_2O/reduced graphene oxide composites for the photocatalytic conversion of CO_2. ChemSusChem 7(4):1086–1093
28. Mei L, Feng J, Wu L, Chen J, Shen L, Xie Y, Wang A (2016) A glassy carbon electrode modified with porous Cu_2O nanospheres on reduced graphene oxide support for simultaneous sensing of uric acid and dopamine with high selectivity over ascorbic acid. Microchim Acta 183(6):2039–2046
29. Wu S, Fu G, Lv W, Wei J, Chen W, Yi H, Gu M, Bai X, Zhu L, Tan C, Liang Y, Zhu G, He J, Wang X, Zhang K, Xiong J, He W (2018) A single-step hydrothermal route to 3D hierarchicalCu_2O/CuO/rGO nanosheets as high-performance anode of lithium-ion batteries. Small 14(5):1702667–1702675
30. Yuan F, Ding L, Li Y, Li X, Fan L, Zhou S, Fang D, Yang S (2015) Multicolor fluorescent graphene quantum dots colorimetrically responsive to all-pH and a wide temperature range. Nanoscale 7(27):11727–11733
31. Kuo C, Chen C, Huang M (2007) Seed-mediated synthesis of monodispersed Cu_2O nanocubes with five different size ranges from 40 to 420 nm. Adv Funct Mater 17(18):3773–3780
32. Chen X, Jin Q, Wu L, Tung C, Tang X (2014) Synthesis and unique photoluminescence properties of nitrogen-rich quantum dots and their applications. Angew Chem Int Ed 53(46):12542–12547
33. Sun H, Li X, Li Y, Fan L, Kraatz HB (2013) A novel colorimetric potassium sensor based on the substitution of lead from G-quadruplex. Analyst 138(3):856–862
34. Gao L, Zhuang J, Nie L, Zhang J, Zhang Y, Gu N, Wang T, Feng J, Yang D, Perrett S, Yan X (2007) Intrinsic peroxidase-like activity of ferromagnetic nanoparticles. Nat Nanotechnol 2(9):577–583